



# Evaluation of Empirical SPT N-Vs Correlations Using 1D Site Response Analysis for Shallow Bedrock Sites in Islamabad, Pakistan

Muhammad Aaqib<sup>1</sup> · Van-Quang Nguyen<sup>2</sup> · Omer Javaid<sup>3</sup> · Ali Hamaiz Khan<sup>1</sup> · Muhammad Aaliyan Ashraf<sup>1</sup> · Bikram Bhusal<sup>4</sup>

Received: 9 January 2024 / Accepted: 4 September 2024  
© The Author(s), under exclusive licence to Shiraz University 2024

## Abstract

The use of standard penetration test blow count (SPT- N) to obtain shear wave velocity (Vs) profiles in the absence of geophysical field test data is a common practice. This study uses a set of SPT-N profiles from Islamabad, Pakistan, to develop Vs profiles using empirical SPT-N and Vs empirical correlations. A set of SPT-N and Vs correlations based on the frequency of their use for seismic site response studies in the region were selected. A suite of one-dimensional site response analyses is then performed on the generated Vs profiles. The 13 input ground motions were chosen to be compatible with the site class B of the newly enacted building code of Pakistan (BCP 2021). A set of 546 1D nonlinear site response analyses were carried out and site response outputs were compared with the corresponding design spectra of the building code of Pakistan. The site-specific comparisons revealed that the calculations of region-specific empirical correlations are more compatible with the code design spectrum for site class C, whereas the outputs using empirical correlations of other regions are more compatible with the code design spectrum for site class D. Based on a comparative analysis, suitable empirical correlations for engineering practices in Islamabad, Pakistan are recommended.

**Keywords** One-dimensional Nonlinear site Response Analysis · SPT N – Vs Correlation · Design Spectrum · Shallow Bedrock Sites · BCP 2021

## 1 Introduction

Pakistan is an earthquake-prone country. Geologically, Pakistan is situated on the Eurasian and Indian plates. The capital city of Pakistan, Islamabad, is located right at the edge of the Potohar Plateau at 33.43 N, 73.04 E. Islamabad was hit by a strong earthquake with a moment magnitude ( $M_w$ ) of 7.8 on October 8, 2005. More than 250 people were buried

alive, and over 74,000 died due to that deadliest earthquake (Mahmood et al. 2016).

The study of the hazards related to earthquakes plays an important role in the sustainable development of Pakistan. Particularly in highly vulnerable regions like Islamabad since it varies from sector to sector (Bhatti et al. 2011). To predict ground shaking intensity in the form of surface motions during earthquakes and to practice safe building design, ground response analysis is usually performed (Aaqib et al. 2020; Nguyen et al. 2020; Seyhan and Stewart 2014). Vs is a fundamental parameter required to perform seismic ground response analysis and seismic site classification (Aaqib et al. 2018, 2021, 2022; Bhusal et al. 2022; Tran et al. 2021). Time-averaged Vs of the top 30 m ( $V_{s30}$ ) is one of the fundamental parameters for seismic site classification systems in the building codes around the world (BSSC 2015; EC8 2005), including Pakistan (BCP 2021) (hereafter referred to as Code). Vs is typically measured by using in-situ seismic non-destructive tests. However, there is a lack of such tests due to cost limitations. Standard Penetration Test (SPT) is the most common in-situ test conducted in

✉ Van-Quang Nguyen  
nguyenvanquang240484@gmail.com

<sup>1</sup> Department of Civil Engineering, National University of Technology, Islamabad, Pakistan

<sup>2</sup> Department of Civil Engineering, Vinh University, Vinh, Vietnam

<sup>3</sup> College of Civil and Transportation Engineering, Shenzhen University, Shenzhen, China

<sup>4</sup> Durham School of Architectural Engineering and Construction, University of Nebraska-Lincoln, Omaha, NE, United States

Pakistan. Therefore, the empirical correlations between in-situ SPT-N measurements and  $V_s$  are utilized to determine the  $V_s$  profiles. Extensive research has been performed in this regard resulting in the development of a number of empirical correlations (Ahmad et al. 2015; Lee 1990) (hereafter referred to as AEA15 and L90, respectively). Most of the empirical correlations have been developed using uncorrected SPT-N values.

Some studies have utilized the SPT N- $V_s$  correlations in Pakistan for ground response analyses. Mahmood et al. (2016) used the empirical correlation of L90 to study the one-dimensional site response to the Margalla tower collapse in Islamabad. Analysis was performed using DEEPSOIL on the data from various laboratory tests for 21 m deep soil layers of type silty clay, and lean clay. The  $V_s$  values calculated by L90 closed in on the average  $V_s$  of the site, as they conformed to range of site class C. Mahmood et al. (2020) used a suite of empirical correlations to perform the site-specific ground response at the Peshawar cultural museum. They used 6 correlations proposed by different researchers for different soil locations and calculated an average value for one-dimensional response analysis on a 10 m deep borehole. Employed two methods, equivalent linear and nonlinear to compare for comparative results. Lodi et al. (2015) used the empirical correlation of Anbazhagan et al. (2013) to develop a functional form for  $V_{s30}$  with depth. They probed the relationship between  $V_s$  of shallow bore log with  $V_s$  of top 30 m soil at Karachi for 1490 bore logs dataset. Since the correlation between SPT-N  $V_s$  varies regionally, and no specific studies exist for Pakistan soil, a study from north India which offered high goodness of fit was used. Sadiq et al. (2021) used the correlation of L90 to evaluate the site amplification factors of Islamabad, Pakistan. To characterize soil, they selected six soil profiles for one dimensional site response analysis. The study highlighted the inadequacy of the previous code, which was based on the Western United States. The correlation of L90 was used, as it generates  $V_s$  profiles that closely match the average  $V_s$  profile for Islamabad.

In all the above-mentioned studies, the evaluation of the empirical correlations was not investigated before using them for site response analyses. The chosen correlations were based on their ability to generate  $V_s$  profiles, which closely matched with  $V_s$  of the site or the goodness of fit for their respective regions. This raises concerns, as some correlations might underestimate, or overestimate ground motion compared to the design expectations of the Code. This makes evaluation necessary because some empirical correlations might produce a response spectrum that underestimates or overestimates the Code design. There is a need to evaluate the existing correlations in context to the Code to perform a reliable site response analysis. It is also worth

mentioning that the Code has recently been updated in 2021, and there is a need to evaluate these correlations in the context of the Code. In this study, six different correlations from the literature were selected based on their frequency of use in the region. These correlations were then used to develop the  $V_s$  profiles from SPT-N values of the six representative profiles from a dataset of 62 profiles. A suite of 1D nonlinear site response analyses was performed on the six sets of profiles, and comparisons were made with the Code by comparing amplification factors,  $F_a$  and  $F_v$ , and design spectra for respective site classes, percentage differences of outputs for each correlation of this study with the code. Based on an extensive comparative analysis with Code, suitable correlations for use in site response analyses in Islamabad were recommended. Figure 1 demonstrates the methodology of the analyses adopted in this study.

## 2 A Review of the Building Code of Pakistan (BCP 2021) and Existing SPT N- $V_s$ Correlations used

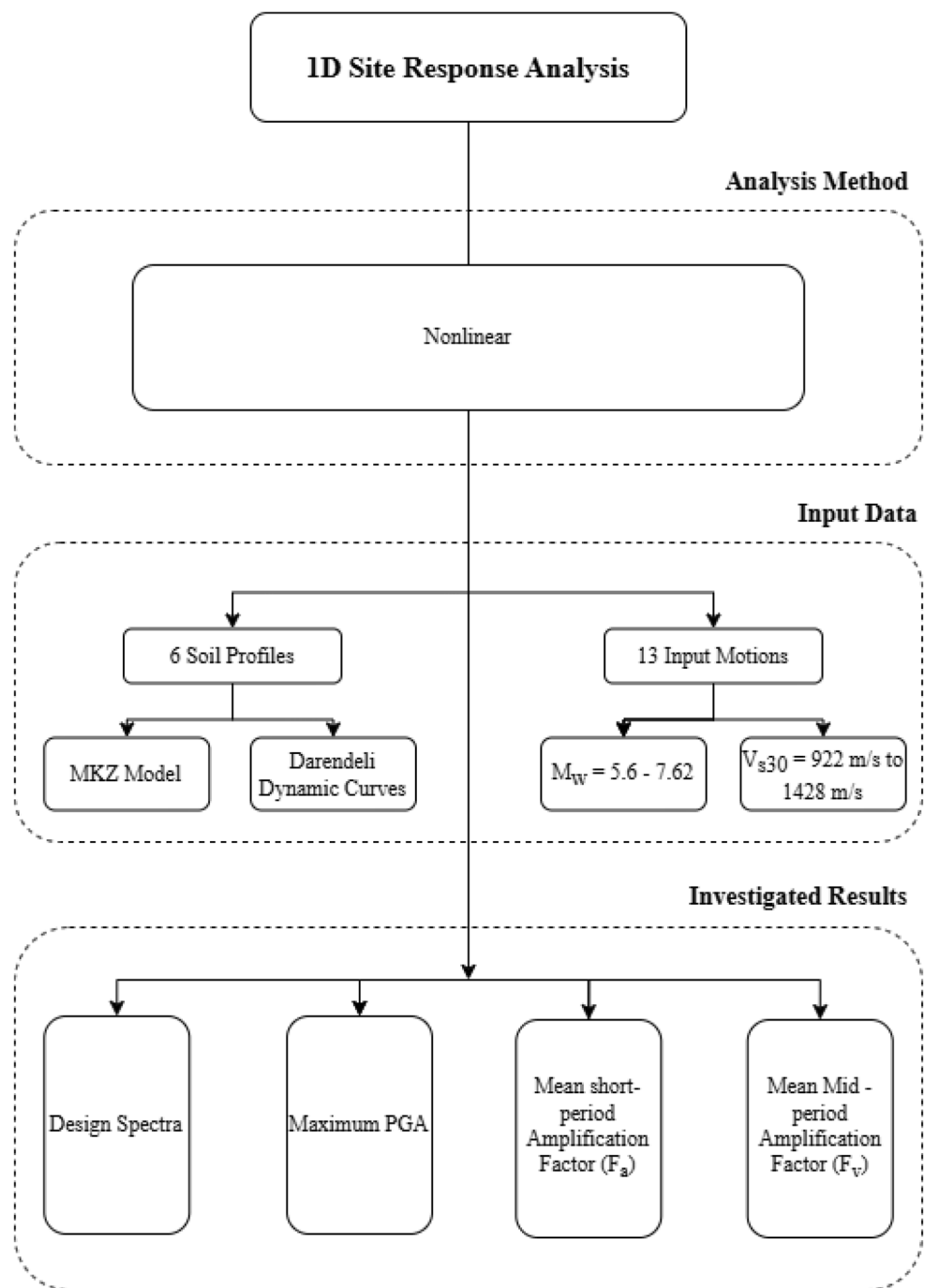
The current seismic provisions in the Code are in accordance with (ASCE 7). In the Code, based on Probabilistic Seismic Hazard Analysis (PSHA), mapped spectral acceleration of short period at 2% probability of exceedance in 50 years ( $S_S$ ) and mapped spectral acceleration of long period at 2% probability of exceedance in 50 years ( $S_1$ ) are important parameters in seismic design. Sites are classified into five classes based on  $V_{s30}$ . Soil classification is summarized in Table 1. The characterization of the design spectrum is illustrated in Fig. 2. The design spectral response acceleration values for short periods ( $S_{DS}$ ) and for a 1-second period ( $S_{D1}$ ), are determined as follows:

$$S_{DS} = \frac{2}{3} \cdot S_{MS} = \frac{2}{3} \cdot F_a \cdot S_S \quad (1)$$

$$S_{D1} = \frac{2}{3} \cdot S_{M1} = \frac{2}{3} \cdot F_v \cdot S_1 \quad (2)$$

where:  $S_S$  is the mapped maximum considered earthquake spectral response acceleration at short periods,  $S_1$  is the mapped maximum considered earthquake spectral response acceleration at a period of 1-second ( $S_S$  and  $S_1$  are determined from hazard map),  $F_a$  is the short-period amplification factor, and  $F_v$  is the long-period amplification factor.

This section also reviews the correlations often used for site response analyses in the Islamabad-Rawalpindi region for the main reason these correlations are selected for the analysis of this study. AEA15 performed a set of seismic cross-hole tests to measure  $V_s$  across 86 sites in the Mardan

**Fig. 1** Methodology flowchart implemented in this study

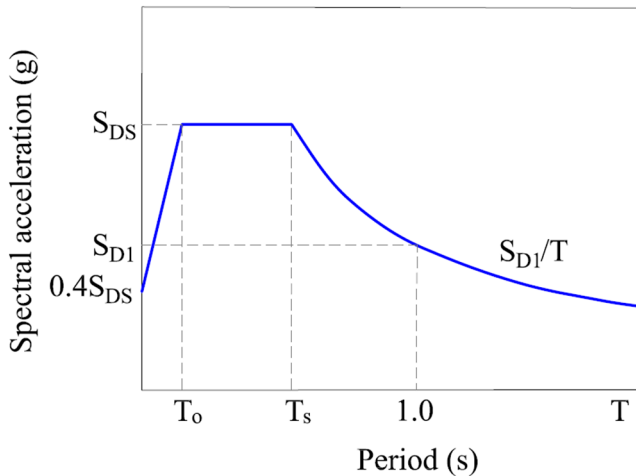
region. A total of 86 SPT-N were also performed at similar sites. Two SPT N-Vs correlations were proposed, with one of them being a function of depth and SPT-N, whereas the other was a function of SPT-N only. For consistency with other correlations used in this study, the function dependent on SPT-N only is used for the development of Vs profiles in this paper.

Anbazhagan et al. (2012) (hereafter referred to as A12) performed a comprehensive review of the existing empirical relationships between shear modulus ( $G_{\max}$ ) and SPT-N

values, and developed a new relationship using new data and the data available in the literature. The authors showed that most previous relationships were based on assumed or extrapolated data, constant density values, and a 78% SPT hammer energy, which is probably unsuitable for other regions and soil types. The new correlation, generated using measured data from Japan and India by A12, combined new data gathered by the authors with old available data. The resulting correlation had a higher coefficient of regression and a lower standard error.

**Table 1** Seismic site classification according to Code

Site	Description	$V_{s30}$ (m/s)	SPT-N	Undrained shear strength, $S_u$ (kPa)
$S_A$	Hard rock	> 1500		
$S_B$	Rock	760–1500		
$S_C$	Very dense soil/ Soft rock	360–760	> 50	> 100
$S_D$	Stiff soil	180–360	15–50	50–100
$S_E$	Soft soil	< 180	< 15	< 50
$S_F$	The soil requires site-specific evaluation			

**Fig. 2** Characterization of the design spectrum in Code

L90 conducted a study to examine the theory and parameters of  $V_s$  for various soil types in the Taipei basin. The study found that existing regression equations were not suitable for Taipei basin soils due to their unique sedimentary environments and soil types. To address this, the study suggested including soil type and geologic effects when developing regression models for estimating  $V_s$ . The study recommended using depth as the primary parameter instead of the SPT-N. The results showed that the regression equations developed by the study were reliable and had high correlation coefficients. A total of 88 data sets from 15 boreholes in the Taipei basin were used, covering a depth of measurement of 680 m.  $V_s$  was calculated using the travel time and distance of the shear wave between two geophone locations. SPT was used to obtain the N-value, a measure of soil resistance. The study concluded that the proposed regression models were rational and reliable for estimating  $V_s$  in the Taipei basin. The study also highlighted the importance of considering soil type and geologic effects when developing regression models for estimating  $V_s$ .

Mhaske and Choudhury (2011) (hereafter referred to as MC11) conducted a study in Mumbai, India, to develop a correlation between the SPT-N and  $V_s$  for different soil types. They gathered data from over 400 soil borehole data

points across the city. The proposed correlation was compared with other correlations from different Indian cities. Based on the developed  $V_s$  profiles, geospatial contour maps of  $V_s$  for Mumbai city were generated to help designers and practitioners in the seismic studies involved in geotechnical engineering.

Imai and Tonoughi (1982) (hereafter referred to as IT82) investigated the relationship between SPT-N and  $V_s$  for different soil types in Japan. They found that existing empirical correlations were not suitable for Japanese soils. The PS logging method was used to characterize the properties of the borehole wall and the surrounding rock. The study derived empirical correlations specific to clayey, silty, and sandy soils in Japan, which were found to be accurate and reliable. The researchers used SPT to obtain the N-value and cross-hole tests to measure  $V_s$  in situ. They analyzed 102 data sets from 400 boreholes in areas throughout Japan.

Ohta and Goto (1978) (hereafter referred to as OG78) used four characteristic indices: SPT-N, depth, geological period, and soil type for the development of empirical correlations. These four indices were combined to produce fifteen correlations for the theoretical estimation of low-strain  $V_s$ . The equations were derived using about 300 data sets, most of which were from alluvial plains in Japan. The authors used a quantification technique that extended the work of Hayashi (1961) to solve a system of simultaneous linear equations comprising both metric (such as SPT-N, depth, and  $V_s$ ) and non-metric variables (such as geological age and soil type). They also undertook a preliminary transformation of the variables to identify a function that closely approximated a linear relationship between the metric variables and  $V_s$ .

Ijaz et al. 2022 (hereafter referred to as IEA22) is an extension of the research with regards to mega-district Lahore and is a part of the research efforts to extent unique Geotechnical Soil Maps (GSMs) corresponding on the base of GEE platform. IEA22 utilized Inverse Distance Weighting (IDW) interpolation, where an improved variant of the modified Shepard method was used. The key geotechnical parameters assessed in the study region are soil consistency, stiffness and activity at various depths. The soil apparently consisted mostly of fine-grained deposits at shallow depths and higher bearing values and non-active soils at depths beyond 3 m. The GEE based IDW algorithm provides effective performance in accurate map generation.

Ijaz et al. 2023 (hereafter referred to as IEA23) showed the soil composition in its natural state by creating geotechnical maps (GMs) from the large-scale dataset obtained from the test results of field and lab. The essential parameters like  $V_s$ , SPT-N, PI and  $\Phi$  were used to create the maps. IDW and shepherd method were found out to be the most accurate for computing the interpolated values between two values of

the dataset. The resulting maps showed that the top layers of soil (from 1.5 to 3 m deep) were mostly fine-grained, with SPT-N and  $V_s$  values between 0 and 20 and 0 and 300 m/s, respectively. The deeper layers (more than 3 m deep) were mostly coarse-grained soil, cobbles, and boulders. Everything was within the acceptable limits by the Code at 1.5 m depth, while IEA23 analyzed the chemical composition of the soil along with confirmation of the results with some statistical analyses performed illustrated on the maps. Recommendations were outlined by IEA23 for the areas that might be problematic for foundation design with the help of a map.

Hassan et al. 2022 (hereafter referred to as HEA22) conducted spatial interpolation techniques for constructing soil zonation maps (SZM) for Islamabad, Pakistan, from the dataset of 210 geotechnical reports obtained from field and lab testing considered soil type, SPT-N values, undrained shear strength, and consolidation parameters. Ordinary kriging interpolation was used in ArcGIS software to generate SZMs based on SPT-N values and soil types that served as a foundation for evaluating settlement and allowable bearing capacity (ABC) for shallow foundations. The study area based on the findings were categorized into three primary zones based on SPT-N values and six sub-zones based on lithology of soil in which lean/silty clay dominated the upper 15 m, transitioning below up to 50 m gravel and shale/sandstone. HEA22 further presented correlations derived through linear regression analysis with an R-squared value of 0.98, enabling the prediction of SPT-N with respect to depth. The investigation concluded that the ABC for shallow foundations in Islamabad surpassed 100 kPa, signifying a highly favorable scenario for supporting the foundations of lightly loaded structures. Moreover, the established correlation for predicting SPT-N values demonstrated exceptional accuracy, achieving approximately 85% and 94% for SPT-N and soil type, respectively.

Ijaz et al. 2021 (hereafter referred to as IEA21) used SMs to create a comprehensive picture of the subsurface soil properties in Sialkot, Pakistan by analyzing large scale dataset from field and laboratory tests by investigating factors including soil type, consistency, and strength at different depths, from which it was concluded that up to 3 m depth the soil was dominated by fine-grained soil with a PI between 7 and 17. This fine-grained soil had a  $V_s$  of 138 to 195 m/s and SPT-N values between 2 and 8. Below 3 m, the

soil transitioned to a non-plastic coarse-grained type with SPT-N values ranging from 8 to over 16 and  $V_s$  exceeding 232 m/s. IEA21 developed correlations using linear regression analyses to predict soil strength and consistency based on depth that resulted in good accuracy, with a coefficient ranging from 82 to 94% for predicting both SPT-N values and PI.

The empirical correlations used in this study are summarized in Table 2. These empirical correlations were chosen from the literature explained in the previous sections based on their frequency of use for seismic site response studies in the region. It is worth mentioning that most of the studies proposed several correlations. Therefore, the correlations that resulted in the highest correlation coefficient and recommended by the authors were used in this study.

### 3 Site Profiles

A total of six representative profiles are utilized in this paper. Representative profiles were selected based on 62 boreholes data drilled across the Islamabad-Rawalpindi region. The soil profile analysis conducted in Islamabad highlights a varied distribution of soil types, particularly clay and silty clay, spanning different depths. The current soil profile data strongly supports and confirms the prevalence of clay and silty clay within the region, echoing the conclusions drawn in the earlier studies.

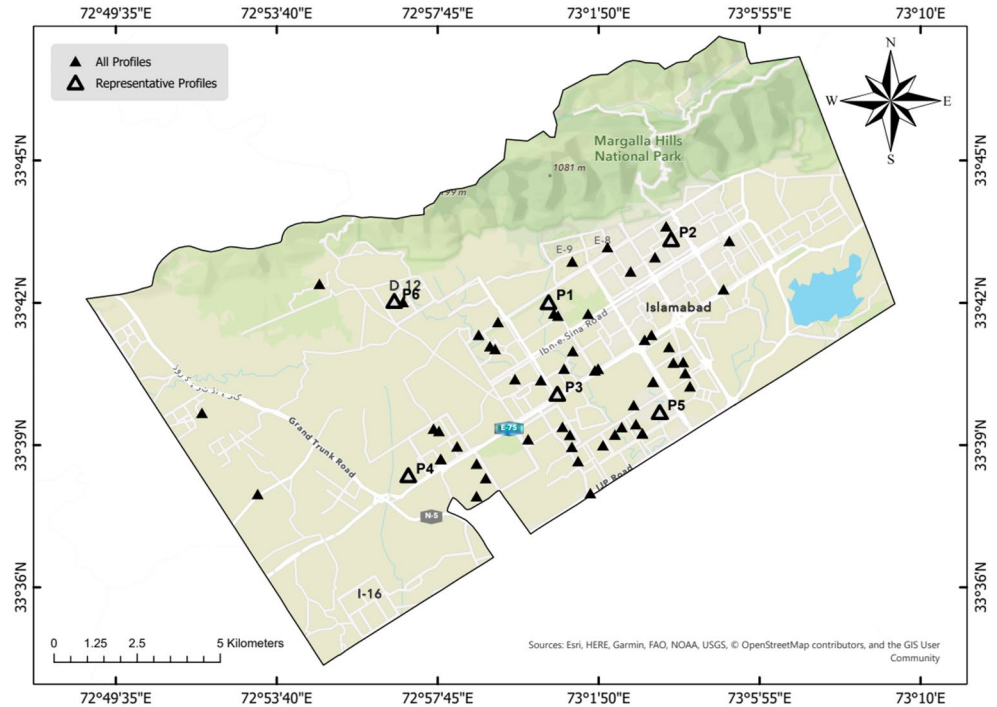
Moreover, these studies not only confirm the existence of these soil types but also detail their distribution patterns. Clay dominates at shallower depths, gradually transitioning into silty clay at deeper levels. This consistent correspondence between the present observations and prior scholarly research highlights the reliability and strength of the data, providing a comprehensive understanding of Islamabad's soil profile.

The locations of the available boreholes and the representative profiles are shown in Fig. 3. The selected profiles have a depth to bedrock (H) ranging from 5 m to 50 m, as demonstrated in the available borehole data. Figures 4 and 5 illustrate the developed  $V_s$  profiles using the correlations explained in Sect. 2. The stratigraphy of each profile is also shown in Figs. 4 and 5. The use of correlations resulted in the development of a wide range of  $V_s$  profiles which is attributed to the fact that these correlations are developed for different regions of the world. A total of 36  $V_s$  profiles were generated using six representative profiles and six SPT N- $V_s$  correlations. It should be noted that the mean of the  $V_s$  profiles (hereafter referred to as MP) developed for each representative profile was also used for the site response analyses, making the total number used for analyses to be 42. The bedrock was considered at 760 m/s as per the

**Table 2** Empirical correlations used in this study

No.	Study	Correlation
1	AEA15	$V_s = 171.02 N^{0.263}$
2	A12	$V_s = 106.63 N^{0.39}$
3	L90	$V_s = 114.43 N^{0.31}$
4	MC11	$V_s = 72 N^{0.4}$
5	IT82	$V_s = 72 N^{0.4}$
6	OG78	$V_s = 85.35 N^{0.348}$

**Fig. 3** Locations of boreholes and representative profiles used in this study



recommendations of Mahmood et al. (2016); Sadiq et al. (2021) for the Islamabad-Rawalpindi region.

Table 3 summarizes the site characteristics of the developed profiles.  $V_{s30}$  of the strata was calculated as follows:

$$V_{s30} = \frac{30}{\sum_{i=1}^{30} \frac{d_i}{V_{si}}} \quad (3)$$

The natural period of the soil profile ( $T_G$ ) is the fundamental parameter that corresponds to the natural frequency of the site.  $T_G$  was determined through:

$$T_G = 4 \sum_{i=1}^{30} \frac{d_i}{V_{si}} \quad (4)$$

$V_{s30}$  of the developed profiles ranged from 227 m/s to 597 m/s, whereas  $T_G$  ranged from 0.098 s to 0.656 s providing valuable information for seismic hazard assessment. Higher  $V_{s30}$  values (597 m/s) suggest stiffer soil conditions, which tend to amplify lower frequency ground motions during earthquakes resonating with shorter TG values, while lower  $V_{s30}$  values (227 m/s) signify softer soils that may amplify higher frequency tremors resonating with longer TG values. This data helps assess the potential impact of earthquakes on various structures at the site. Buildings with natural frequencies close to the predominant ground motion frequencies (related to  $V_{s30}$  and TG) are more susceptible to damage.

As per Code, 30 classes were classified as site class C (hereafter referred to as  $S_C$ ), whereas 12 sites were classified

as site class D (hereafter referred to as  $S_D$ ). This classification is attributed to the shallow nature of site profiles in the Islamabad-Rawalpindi region, which was also reported by (Adeel et al. 2023; Mahmood et al. 2016; Sadiq et al. 2021).

## 4 Site Response Analysis

A total of 13 input ground motions were selected from NGA-west 2 (<https://ngawest2.berkeley.edu/>) database. The input ground motions were selected such that they are compatible with the design spectrum of  $S_B$  in Code. The ground motions were scaled to a peak ground acceleration (PGA) of 0.31 g, which is the ground motion level at 2% probability of exceedance in 50 years corresponding to an annual return period of 2475 years for Islamabad according to the Code. Figure 6 illustrates the suite of scaled input ground motions along with the Code design spectrum of  $S_B$ . The details of input ground motions are summarized in Table 4. The scaling was performed in line with the procedures outlined in ASCE 7–10 (Charney 2015).

A total of 546 1D nonlinear site response analyses were performed using DEEPSOIL (Hashash et al. 2017). The pressure-dependent Modified Kodner-Zelasko (MKZ) model was used (Matasović and Vucetic 1993). The site-specific dynamic curves were not available. Therefore, the nonlinear modulus reduction ( $G/G_{max}$ ) and Damping curves of Darendeli (2001) were utilized for characterizing the dynamic behaviour of soils under cyclic loading. The modulus reduction curve expresses the ratio of the shear modulus

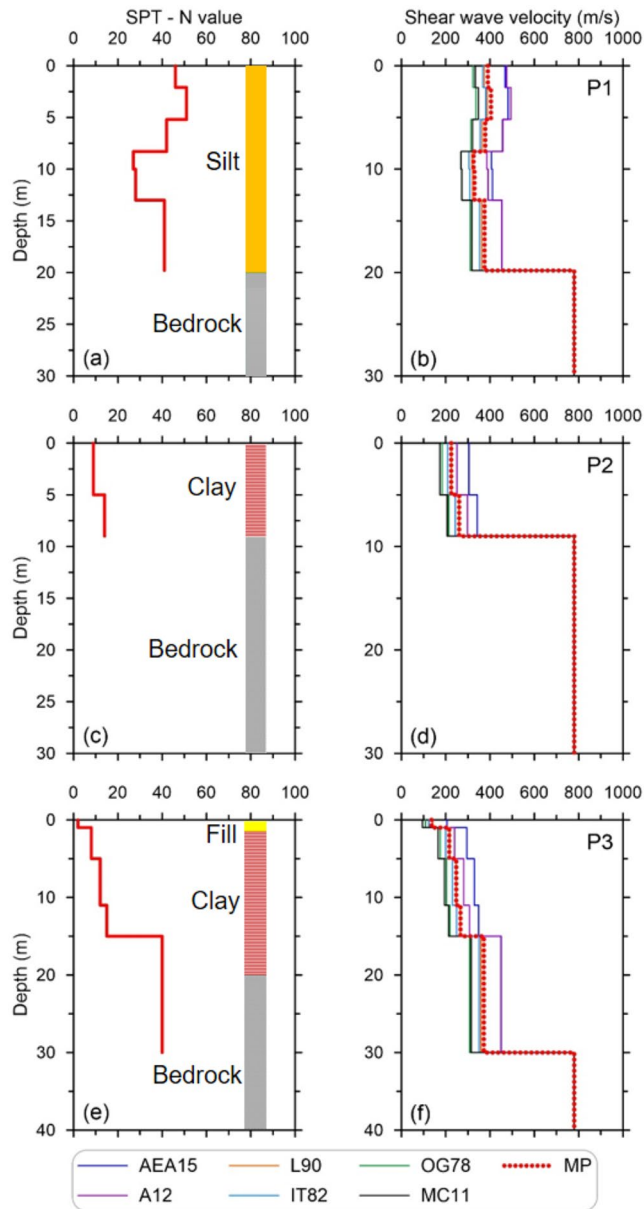


Fig. 4 SPT-N profiles and stratigraphy of the representative profiles along with the developed Vs profiles (P1-P3)

at a given strain ( $\gamma$ ) to the maximum shear modulus ( $G_{max}$ ) as a function of shear strain. The damping ratio curve describes how the damping ratio varies with shear strain. Rayleigh damping is a common approach used in numerical simulations to model damping in structural and geotechnical systems. In the context of small-strain damping, Rayleigh damping is used to represent the inherent material damping in the system at low strain levels. The damping coefficients are typically chosen to match the target damping ratio at certain frequencies of interest. In this study, the 1st and 5th modes were used to calculate the coefficients of Rayleigh damping (Aaqib et al. 2021; Nguyen et al. 2020; Tran et al.

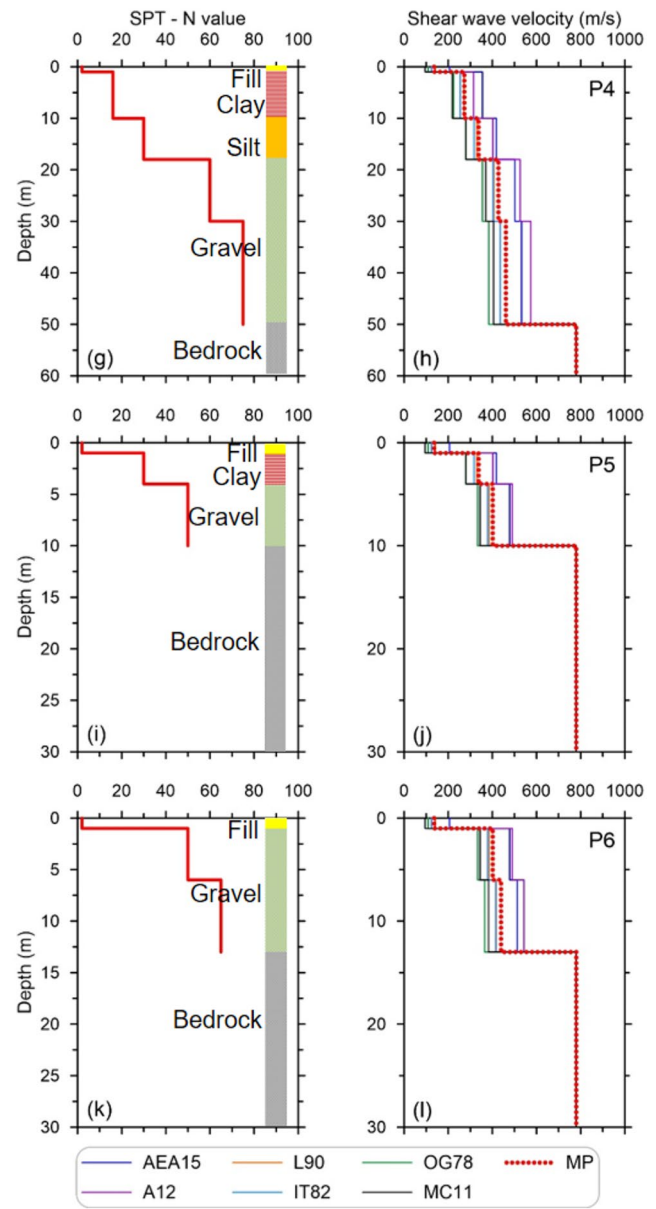


Fig. 5 SPT-N profiles and stratigraphy of the representative profiles along with the developed Vs profiles (P4-P6)

2021). The bedrock was simulated as an elastic half-space due to the outcrop motions used.

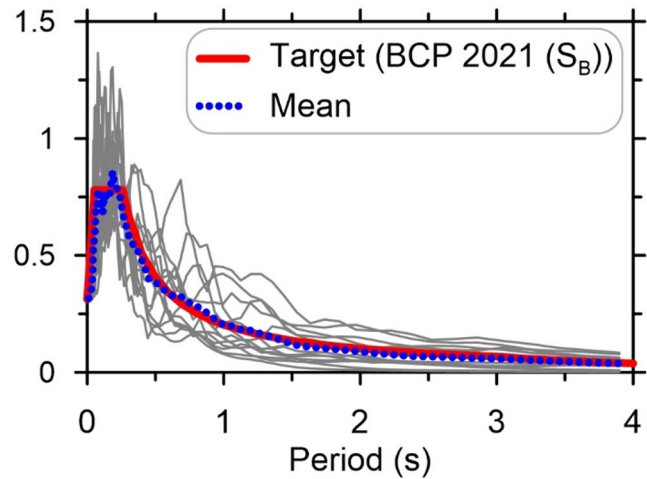
## 5 Results and Discussions

The surface acceleration response spectra and related amplification factors at each period for the 42 site profiles were determined for each rock outcrop input motion. Figure 7 shows the mean calculated response spectra for each representative profile and the corresponding profiles that were developed using the selected SPT N-Vs correlations. Maximum spectral acceleration value was observed at the  $T_G$  of

**Table 3** Characteristics of developed vs profiles

Profile	Correlations	$V_{s30}$ (m/s)	$T_G$ (s)	H (m)	Site class, (BCP 2021)
P1	AEA15	524.07	0.18	19.8	$S_C$
	A12	520.77	0.18	19.8	$S_C$
	L90	436.93	0.22	19.8	$S_C$
	IT82	386.11	0.26	19.8	$S_C$
	OG78	384.93	0.26	19.8	$S_C$
	MC11	391.34	0.25	19.8	$S_C$
	MP	533.58	0.22	19.8	$S_C$
P2	AEA15	545.34	0.11	9	$S_C$
	A12	498.09	0.13	9	$S_C$
	L90	465.41	0.15	9	$S_C$
	IT82	423.82	0.18	9	$S_C$
	OG78	411.52	0.18	9	$S_C$
	MC11	399.51	0.19	9	$S_C$
	MP	451.72	0.16	9	$S_C$
P3	AEA15	368.66	0.33	31	$S_C$
	A12	327.52	0.33	31	$S_D$
	L90	281.59	0.44	31	$S_D$
	IT82	241.38	0.51	31	$S_D$
	OG78	233.49	0.53	31	$S_D$
	MC11	227.29	0.54	31	$S_D$
	MP	270.97	0.30	31	$S_D$
P4	AEA15	409.38	0.44	50	$S_C$
	A12	382.22	0.44	50	$S_C$
	L90	318.55	0.56	50	$S_D$
	IT82	273.49	0.65	50	$S_D$
	OG78	268.09	0.66	50	$S_D$
	MC11	266.27	0.65	50	$S_D$
	MP	310.23	0.57	50	$S_D$
P5	AEA15	597.32	0.10	10	$S_C$
	A12	571.41	0.10	10	$S_C$
	L90	522.49	0.13	10	$S_C$
	IT82	478.67	0.15	10	$S_C$
	OG78	471.51	0.15	10	$S_C$
	MC11	466.68	0.15	10	$S_C$
	MP	513.22	0.13	10	$S_C$
P6	AEA15	590.89	0.12	13	$S_C$
	A12	576.51	0.12	13	$S_C$
	L90	511.87	0.15	13	$S_C$
	IT82	464.14	0.17	13	$S_C$
	OG78	460.11	0.17	13	$S_C$
	MC11	460.48	0.17	13	$S_C$
	MP	505.04	0.15	13	$S_C$

the profiles. The profiles corresponding to P2, P5, and P6 result in the highest response among all the profiles. It is attributed to the presence of strong impedance contrast with the bedrock. Due to the lower estimates of  $V_s$  by OG78, IT82, and MC11, they result in the highest spectral responses for all the profiles at periods  $T < 0.4$  s except P3 and P4. All the corresponding profiles under P3 are  $S_D$ , whereas, 80% of P4 profiles are  $S_D$  sites with low shear wave velocities

**Fig. 6** Suite of scaled input ground motions

generated by all the correlations. AEA15 and A12 result in the highest response for all the  $S_C$  profiles for  $T < 0.2$  s.

Figure 8 illustrates the variation of the mean amplification factor as a function of period. Distinct amplification peaks are observed at the  $T_G$  of all the profiles. For soft profiles P3 and P4, considerable amplification peaks are observed at both short and long periods. For the P3 profile, the stratigraphy shows a fill layer, followed by clay, and finally, bedrock. This is attributed to the fact that the upper softer layers have lower shear wave velocities, i. e.  $V_s = 150$  m/s, which would typically resonate at lower frequencies. As the seismic waves pass through these layers, energy can be trapped and reflected, leading to the amplification observed as the first peak in the spectral acceleration. The second peak corresponds to the deeper layers, particularly the interface of the soil and bedrock. The impedance contrast at this interface is significant, leading to another resonance, which shows up as the second peak in the amplification curve.

Similar to P3, P4 has multiple distinct layers, including fill, clay, and silt, underlain by gravel and bedrock. The spectral amplification for P4 shows multiple peaks because of similar reasons that each layer's resonance can contribute to different peaks of amplification. The impedance contrast between the gravel and bedrock in particular causes strong reflections of seismic waves, contributing to one of the prominent peaks. The first peak in the spectral acceleration is associated with the resonance of the softer, shallower layers, i.e. fill and clay. The second peak is typically due to the deeper, stiffer layers where a significant impedance contrast exists. This contrast results in wave amplification at a different frequency, leading to a second amplification peak. These trends are consistent for the profiles generated by all the correlations. MC11, IT82 and OG78 result in the highest amplification factors for  $T > 0.3$  s, which is primarily attributed to the generation of low shear wave velocities by these

**Table 4** Summary of input ground motions

No	Earthquake name	Year	Station	Mag. ( $M_w$ )	Mechanism	$R_{rup}$ (Km)	$V_{s30}$ (m/s)
1	San Fernando	1971	Cedar Springs_ Allen Ranch	6.61	Reverse	89.72	813.48
2	Tabas_Iran	1978	Tabas	7.35	Reverse	2.05	766.77
3	Coyote Lake	1979	Gilroy Array #1	5.74	Strike-slip	10.67	1428.14
4	Morgan Hill	1984	Gilroy Array #1	6.19	Strike-slip	14.91	1428.14
5	Whittier Narrows-01	1987	LA - Wonderland Ave	5.99	Reverse Oblique	27.64	1222.52
6	Loma Prieta	1989	Gilroy Array #1	6.93	Reverse Oblique	9.64	1248.14
7	Loma Prieta	1989	So. San Francisco_ Sierra Pt.	6.93	Reverse	63.15	1020.62
8	Chi-Chi_Taiwan	1999	ILA063	7.62	Reverse Oblique	61.06	996.51
9	Chi-Chi_Taiwan-02	1999	CHY102	5.9	Reverse	79.68	804.36
10	Chi-Chi_Taiwan-05	1999	TTN042	6.2	Reverse	85.17	845.34
11	Tottori_Japan	2000	HYG004	6.61	Strike-slip	108.34	834.56
12	Tottori_Japan	2000	OKYH02	6.20	Reverse	70.52	1047.01
13	Umbria-03_Italy	1984	Gubbio	5.6	Normal	15.72	922

**Fig. 7** Comparison of calculated mean response spectra for profiles P1-P6

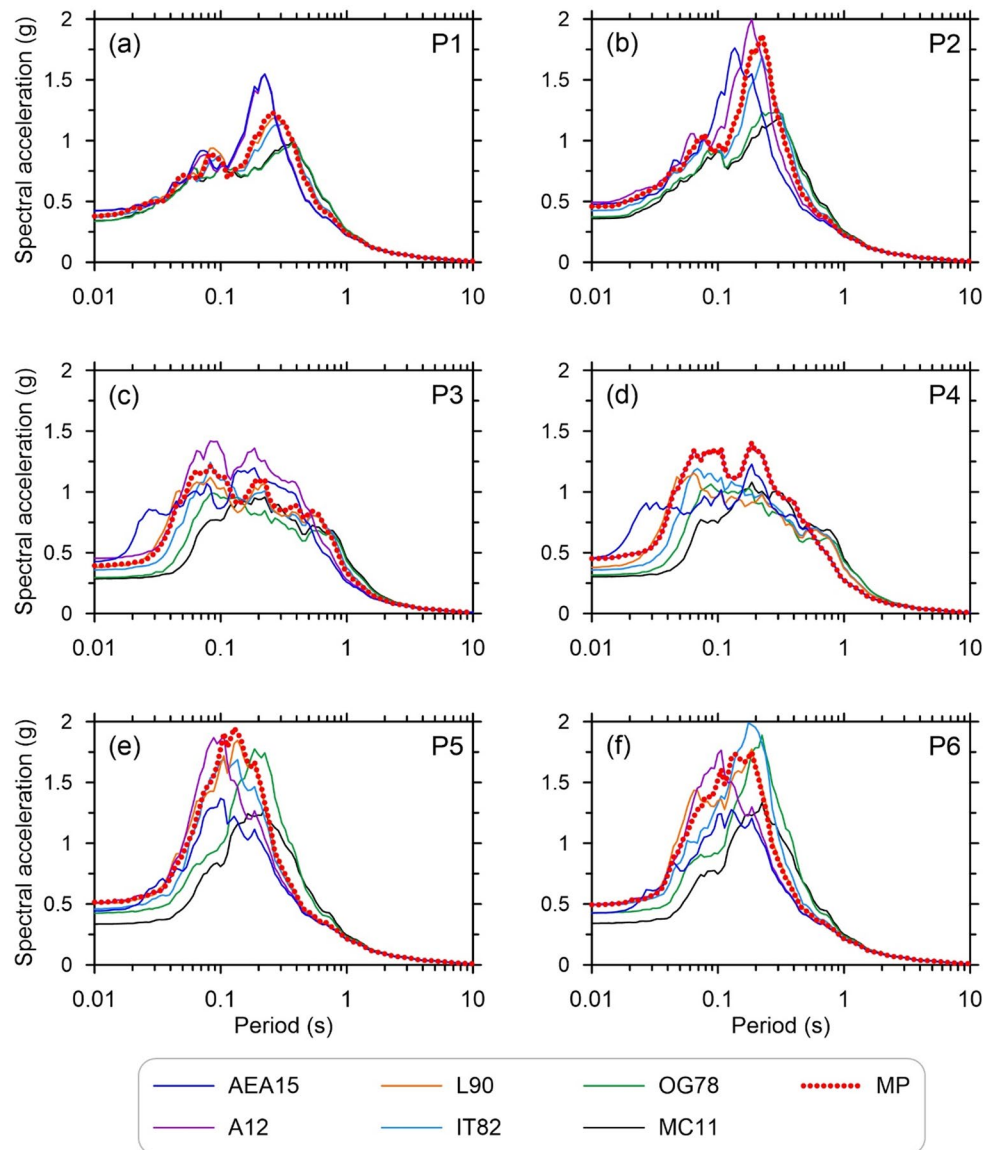
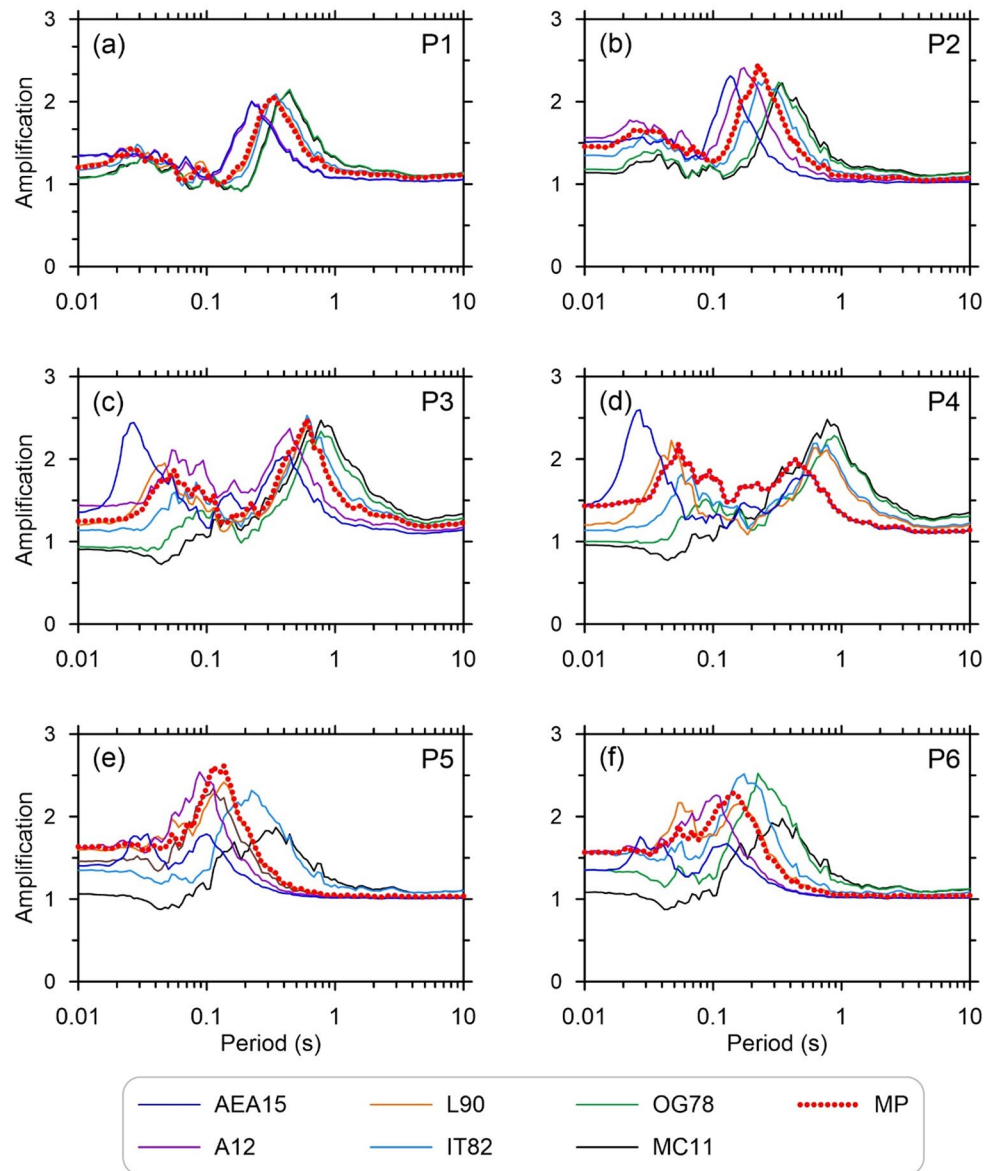


**Fig. 8** Comparison of calculated mean amplification factors for profiles P1-P6



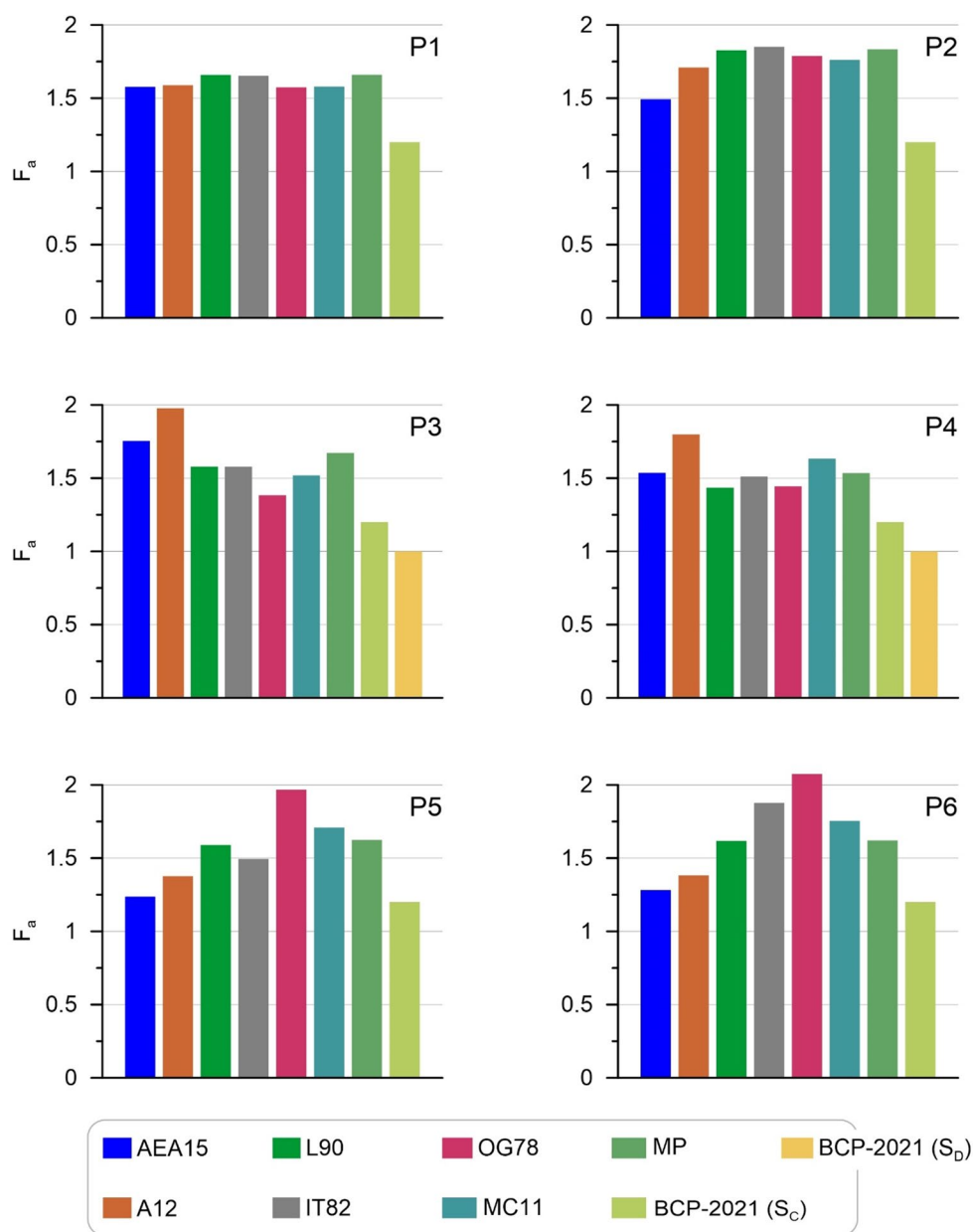
correlations, as compared to the others. For sites corresponding to P1 and P2, no mean amplification was observed beyond 1.5 s. It should be noted that all the sites included in P1 and P2 are  $S_C$  sites, and no long-period amplification was expected. Sites corresponding to P3 and P4 are classified as  $S_D$ ; therefore, a considerable amount of amplification was observed in the period range of 0.4–2.0 s. MC11 results in the highest amplification factor for these sets of sites, which could be due to the relatively softer  $V_s$  profiles developed using this correlation. Sites corresponding to P5 and P6 result in considerable amplification for  $T < 0.5$  s; however, negligible amplification is observed afterward.

### 5.1 Comparison of Calculated $F_a$ and $F_v$ Using Correlations

This section presents the comparison of the calculated  $F_a$  and  $F_v$  with those from the Code. Implications of the observed differences are to explore the site-specific variations from the Code. The design response spectrum plays a fundamental role in achieving resilient and safe structural designs in earthquake-prone regions. The contribution of  $F_a$  and  $F_v$  in the design response spectrum is depicted in Eq. (1) and Eq. (2).

Figure 9 illustrates the comparison of the mean  $F_a$  calculated using the outputs of each correlation.  $F_a$  was calculated using an integration interval of 0.1–0.5 s, which is consistent with the provisions of the Code. P1, P2, P5, and P6 contain  $S_C$  profiles only, whereas P3 and P4 are a mixture

**Fig. 9** Comparison of mean short-period amplification factor ( $F_a$ ) calculated using the outputs of each correlation



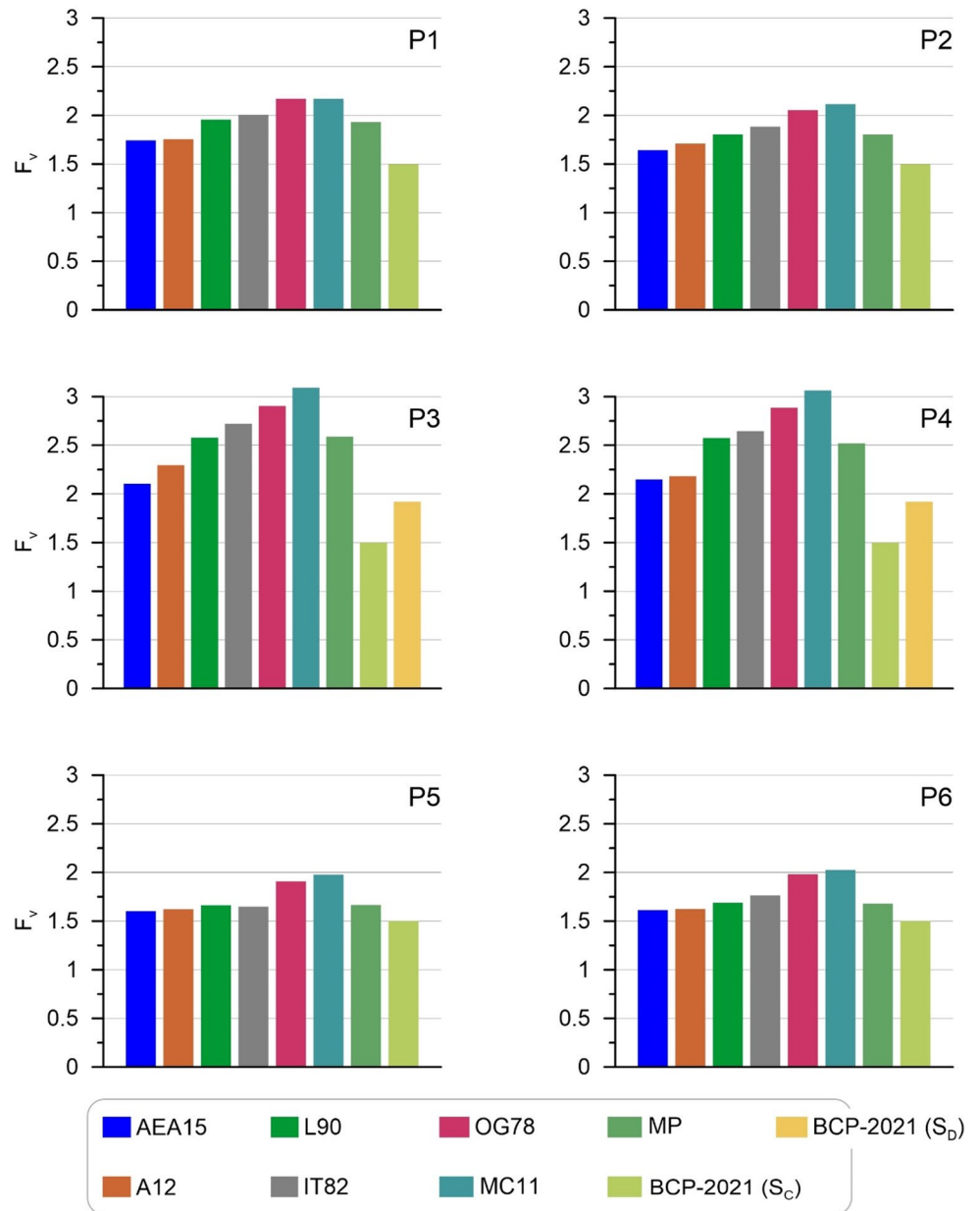
of  $S_C$  and  $S_D$ . For P1, all the correlations result in  $F_a > 1.5$ , which is attributed to the short site periods of profiles ( $T_G < 0.26$  s) in P1. The value of  $F_a$  in Code is 1.2 and 1.0 for  $S_C$  and  $S_D$ , respectively. In the case of P2, AEA15 results in the lowest  $F_a$  among all correlations and is the nearest to the Code value, whereas MP results in the highest value. P3 is a mixture of  $S_C$  and  $S_D$  profiles. OG78 provides the lowest value of  $F_a$  and is closest to the Code value of 1.0 for  $S_D$ , whereas A12 results in the highest value. P4 is also a mixture of profiles classified as  $S_C$  and  $S_D$ . Similar to P3, OG78 produces a  $F_a$  value of 1.45 which is the closest to that of the Code for  $S_D$ . The value of  $F_a$  using AEA15 outputs results in a value of 1.5, which is the lowest to the Code factor of

1.2 for sites classified as  $S_C$ . For P5 and P6, the value of  $F_a$  using AEA15 outputs is similar to the Code factor of 1.2.

Figure 10 presents the comparison of the mean  $F_v$  calculated using the outputs of each correlation.  $F_v$  was calculated using an integration interval of 0.4–2.0 s, which is consistent with the provisions of the Code. The value of  $F_v$  in Code is 1.5 and 1.9 for  $S_C$  and  $S_D$ , respectively. For P1,  $F_v$  calculated using the outputs of AEA15 is nearest to the Code factor with a value of 1.7. OG78 and MC11 results in the highest factor of 2.1.

In the case of P2, AEA15 results in the lowest  $F_v$  among all the correlations and is the nearest to the Code value, whereas OG78 and MC11 results in the highest value. For P3, considerable differences are observed and no correlation

**Fig. 10** Comparison of mean mid-period amplification factor ( $F_v$ ) from site response outputs with code design spectrum



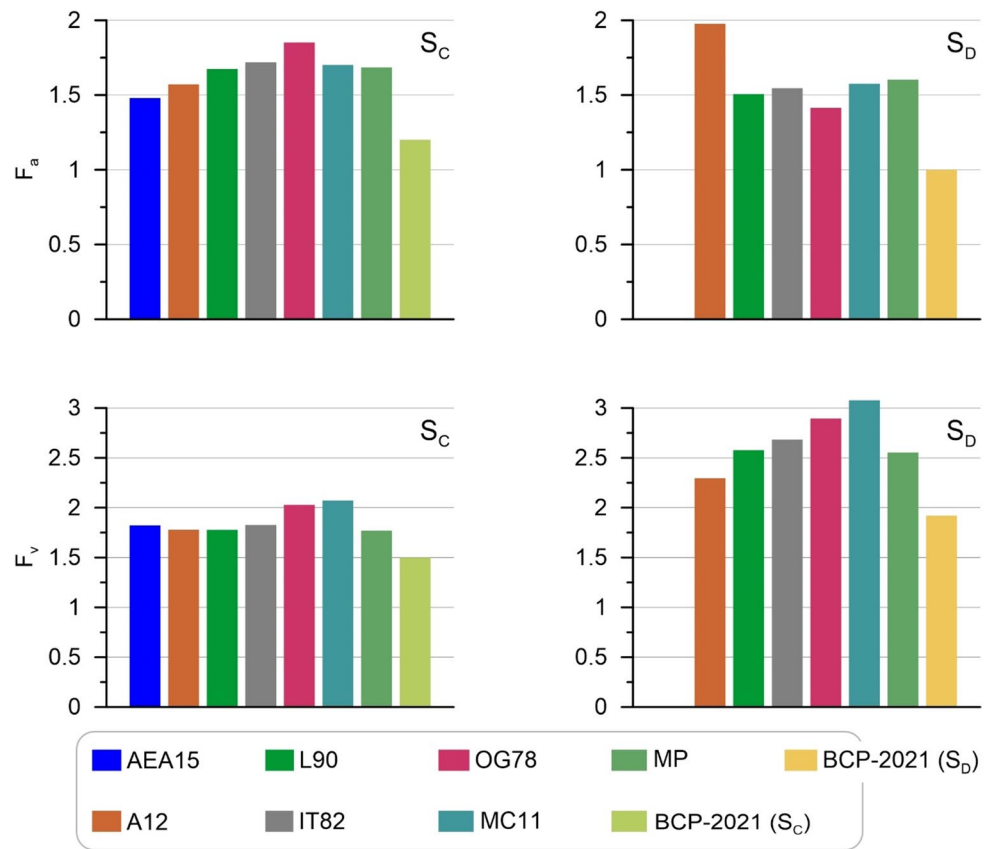
resulted in comparable factors with the Code for both  $S_C$  and  $S_D$ . However, AEA15 resulted in a value nearest to that of Code for  $S_C$ . In the case of P4,  $F_v$  calculated using the outputs of A12 is comparable with the Code factor for  $S_D$ . P5 and P6 do not result in a considerable variation of  $F_v$ , and all the correlations result in a short-period factor consistent with that in the Code except MC11 and OG78, however, AEA15 is demonstrated to be the most consistent. It is worth mentioning that OG78 and MC11 result in higher amplification factors because these correlations result in higher TG values for both  $S_C$  and  $S_D$  profiles. For example, OG78 and MC11 result in the highest  $F_a$  for P5 and P6 which is attributed to a TG of 0.15 and 0.17 s which is the highest among all other correlations if we consider within the integration

interval of 0.1–0.5 s used to calculate  $F_a$ . Similarly, the high  $F_v$  values are attributed to the higher TG values by OG78 and MC11 which effectively captures the amplifications in the integration interval of 0.4–2.0 s.

### 5.2 Comparison of Site Class Specific $F_a$ and $F_v$

Figure 11 demonstrates the  $F_a$  and  $F_v$  calculated by each correlation within a particular site class. There is a variability observed in the case of  $F_a$  for both  $S_C$  and  $S_D$ . For  $S_C$ ,  $F_a$  varies from 1.4 to 1.8, with the outputs of AEA15 resulting in the lowest and that of OG78 resulting in the highest value. Comparisons with the Code  $F_a$  reveal that AEA15 outputs provide a comparable  $F_a$ . In the case of  $S_D$ ,  $F_a$  varies

**Fig. 11** Comparison of site class specific  $F_a$  and  $F_v$



from 1.4 to 1.9. OG78 results in the lowest  $F_a$ , whereas A12 results in the highest.  $F_a$  from OG78 outputs is consistent with the Code  $F_a$ . The variability in  $F_v$  is not considerable the case of  $S_C$  and the factors vary within a narrow band of 1.75–2.05. AEA15 and A12 are shown to be compatible with the Code factors. OG78 and MC11 results in the highest  $F_v$ . In the case of  $S_D$ ,  $F_v$  is the highest for MC11, resulting in a factor of 3.1. The  $F_v$  calculated from A12 outputs is comparable to the code factor.

Figure 12 illustrates the percentage differences between  $F_a$  and  $F_v$  calculated from the outputs of correlations and those in the Code. On the one hand, the short-period amplification generally results in higher percentage differences. The differences in  $F_a$  reveal that AEA15 results in the lowest percentage difference among all the correlations. This trend is consistent across all  $S_C$  profiles. A12 generally results in a lower percentage difference; however, the difference is greater than AEA15. L90 and MC11 result in the highest percentage differences, with a value of up to 60% in the case of MC11. OG78 and IT82 generally produce higher percentage differences except in the case of P4. The MP profile also demonstrates higher differences in all cases except P5 and P6. On the other hand,  $F_v$  is demonstrated to have lower percentage differences as compared to  $F_a$ , except in the case of P3 and P4, where considerable differences were observed. AEA15 results in very low percentage differences, as low as

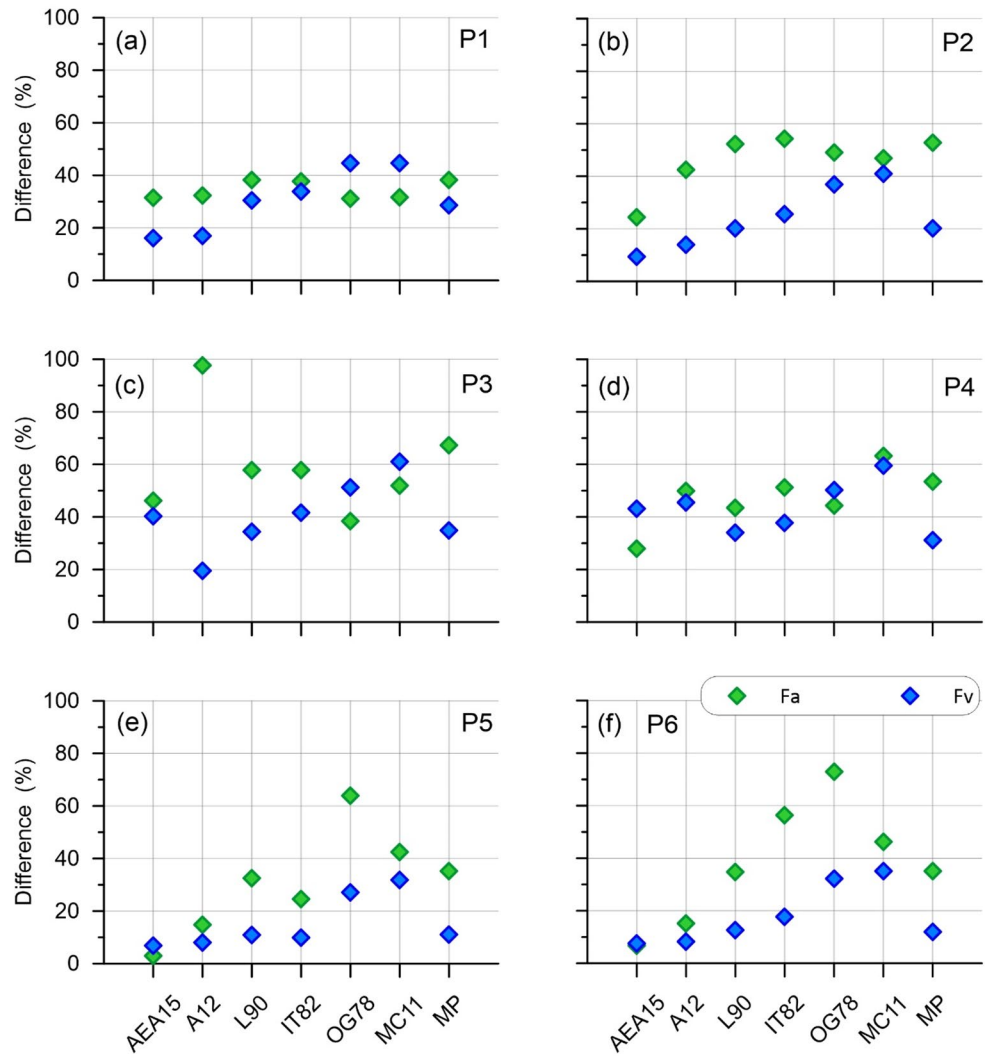
5%, highlighting the applicability of the correlation in the region.  $F_v$  calculated from the outputs of L90, OG78, and MP is also comparable to Code factors and results in lower percentage differences, specifically for  $S_D$  sites.

### 5.3 Comparison of Code Spectra and Site Response Outputs of Correlations

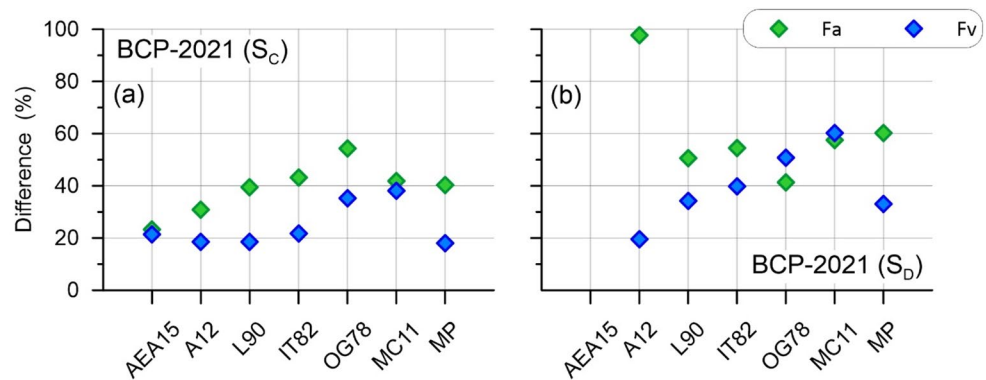
Figure 13 demonstrates the percentage differences within a soil class. AEA15 is shown to demonstrate the lowest differences in site class  $S_C$  for both  $F_a$  and  $F_v$  with percentage differences less than 25%. In the case of site class  $S_D$ , OG78 outputs result in lower percentage differences with values of less than 40% and 50% for  $F_a$  and  $F_v$  respectively. It is worth mentioning that although the comparative analysis reveals low percentage differences for L90, IT82, and MP in the case of  $F_v$ , however, the differences in the case of  $F_a$  are considerable. Therefore, In light of the comparative analysis, it is revealed that AEA15 results are comparable with the Code spectra in the case of site class  $S_C$ , whereas the outputs of OG78 and L90 depict lower differences in the case of site class  $S_D$ .

Figure 14 compares the response spectra developed from the outputs of the correlations with the Code spectra for each set of representative profiles. Comparisons of P1, P2, P5, and P6 demonstrate that the spectra generated using the

**Fig. 12** Percentage difference between site factors calculated from the outputs of correlations and Code factors for  $S_C$



**Fig. 13** Percentage differences calculated using the outputs of each correlation corresponding to Code  $S_C$  and  $S_D$



outputs of AEA15 are comparable with the Code spectra for  $S_C$ . Although AEA15 results in high short-period amplification in case of P1 and P2, however, it is the most comparable with the code. For P3 and P4, there is variability in the spectra because both P3 and P4 contain a mixture of  $S_C$  and  $S_D$  profiles, resulting in the variation of  $T_0$  and  $T_s$  due to a wide range of  $F_a$  and  $F_v$ . Considerable differences were observed

in  $T_0$  and  $T_s$  for P3 and P4. This is primarily attributed to the differences in  $F_a$  and  $F_v$ . Overall, AEA15 is illustrated to be the closest to the Code spectra in the case of  $S_C$ , whereas OG78 and is illustrated to be suitable for  $S_D$ . However, discrepancies were observed specifically at large periods in the case of  $S_D$ .

**Fig. 14** Comparison of Code spectra with those developed using the site response outputs of correlations

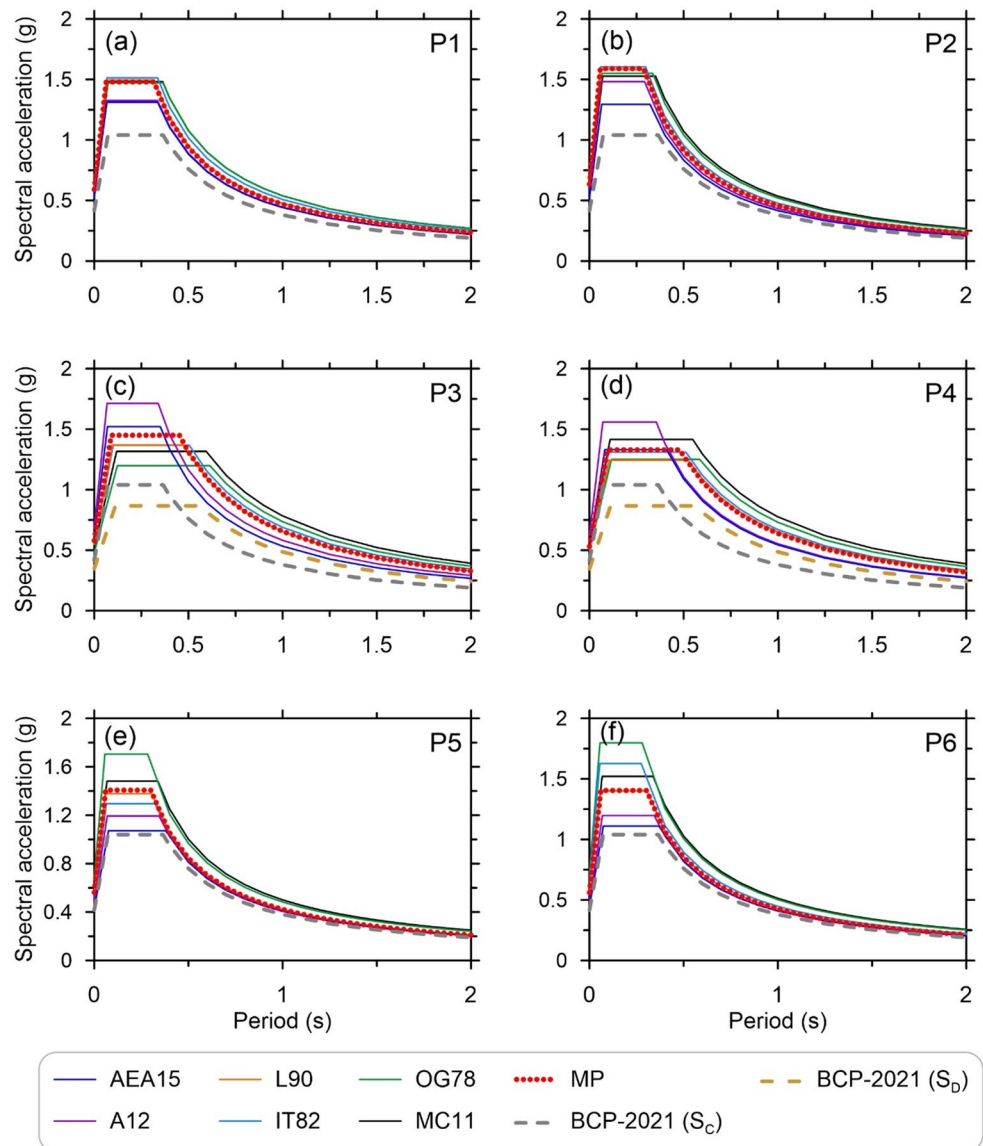
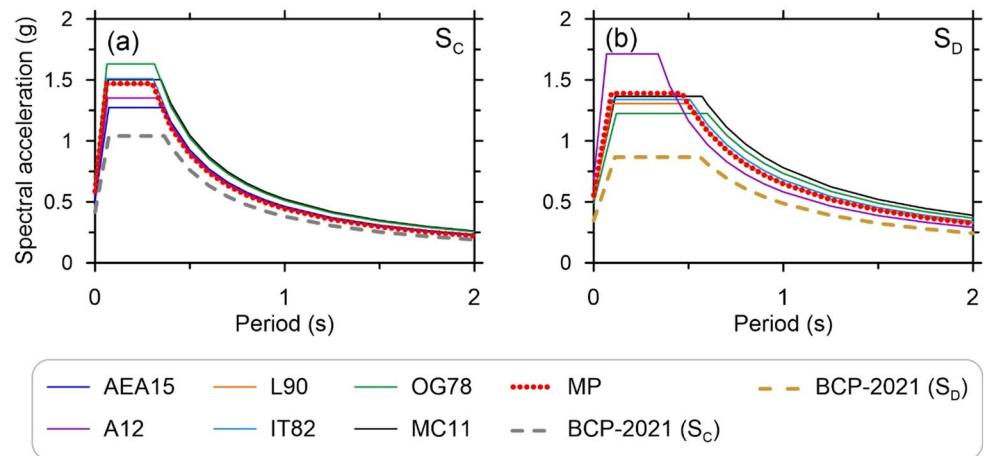


Figure 15 compares the Code spectra with the spectra developed from the site response outputs of the correlations for a particular site class. The comparisons with the  $S_C$  Code spectra reveal that AEA15 results in a Code-compatible spectrum for  $T > 0.7$  s. For short periods, the differences are observed due to higher  $F_a$  calculated by AEA15. All the other correlations result in considerable discrepancies throughout the period range. For  $S_D$ , the spectrum developed from the outputs of OG78 is demonstrated to be the closest to that of Code. At mid to longer periods, the spectrum deviates from the Code spectra. All the other correlations used in this study are considerably different from the Code spectrum throughout the period range.

## 6 Conclusions

This study evaluates empirical SPT N-Vs correlations for shallow bedrock sites in Islamabad, Pakistan. A total of six representative profiles selected from 62 boreholes across the Islamabad-Rawalpindi region are utilized. The  $V_s$  profiles are then developed based on six representative SPT profiles, and six widely used empirical SPT N-Vs correlations were utilized. The 13 input ground motions are chosen to be compatible with the  $S_B$  design spectrum in Code. A set of 546 1D nonlinear site response analyses are carried out using the DEEPSOIL program to obtain the outputs and amplification factors for comparison purposes. The following conclusions can be drawn from the outputs of this study.

**Fig. 15** Response spectra comparison of site classes

1. The maximum spectral acceleration is observed at the natural period of soil profiles developed from selected SPT N-Vs correlations. Generally, among six correlations, the AEA15 results in the lowest response, while OG78 and MC11 produce the highest response.
2. All of the profiles show distinct amplification peaks at the natural period of soil profiles. The amplification is identified in the short period for  $S_C$ , and a considerable amount of amplification is observed in the long period for  $S_D$ . The highest amplification factor is produced by OG78 and MC11 correlations, while the lowest amplification factor is produced by the AEA15. The minimum difference of  $F_a$  between correlations and the Code is found in AEA15 for  $S_C$  and OG78 for  $S_D$ .
3. In general, the outputs of AEA15 are demonstrated to be the most compatible with the Code spectra in the case of  $S_C$ , followed by A12, MP, L90, IT82, and OG78, whereas OG78 is shown to be suitable for  $S_D$ , followed by L90, MP, A12, IT82, and MC11. In the case of  $S_D$ , however, differences are seen to exist, particularly at the long periods.

**Acknowledgements** This study is supported by the Higher Education Commission of Pakistan Ref No. 20-17336/NRPU/R&D/HEC/2021 2021.

**Author Contributions** The authors confirm contribution to the paper as follows: study conception and design: Muhammad Aaqib, Van-Quang Nguyen; data collection: Ali Hamaiz Khan, Muhammad Aaliyan Ashraf; analysis and interpretation of results: Omer Javaid, Bikram Bhusal, Van-Quang Nguyen; draft manuscript preparation: Muhammad Aaqib, Van-Quang Nguyen. All authors reviewed the results and approved the final version of the manuscript.

**Data Availability** No datasets were generated or analysed during the current study.

## Declarations

**Competing Interests** The authors declare no competing interests.

## References

- Aaqib M, Sadiq S, Park D, Hashash YM, Pehlivan M (2018) Importance of implied strength correction for 1D site response at shallow sites at a moderate to low seismicity region. *Geotechnical Earthquake Engineering and Soil Dynamics V: seismic hazard analysis, Earthquake Ground motions, and Regional-Scale Assessment*. American Society of Civil Engineers Reston, VA, pp 445–453
- Aaqib M, Park D, Kim H, Adeel MB, Nizamani ZA (2020) Evaluation of the influence of shear strength correction through a comparative study of nonlinear site response models. *J Korean Geotech Soc* 36(12):77–86
- Aaqib M, Park D, Adeel MB, Hashash Y, Ilhan O (2021) Simulation-based site amplification model for shallow bedrock sites in Korea. *Earthquake spectra, Advance online publication*
- Aaqib M, Park D, Lee Y-G, Pervaiz U (2022) Development of site classification system and seismic site coefficients for Korea. *J Earthquake Eng* 26(16):8257–8279
- Adeel MB, Nizamani ZA, Aaqib M, Khan S, Rehman JU, Bhusal B, Park D (2023) Estimation of V S30 using shallow depth time-averaged shear wave velocity of Rawalpindi–Islamabad, Pakistan. *Geomatics Nat Hazards Risk* 14(1):1–21
- Ahmad I, Waseem M, Abbas M, Ayub U (2015) Evaluation of shear wave velocity correlations and development of new correlation using cross-hole data. *Int J Georesources Environment-IJGE* 1(1):42–51
- Anbazhagan P, Parihar A, Rashmi H (2012) Review of correlations between SPT N and shear modulus: a new correlation applicable to any region. *Soil Dyn Earthq Eng* 36:52–69
- Anbazhagan P, Kumar A, Sitharam T (2013) Seismic site classification and correlation between standard penetration test N value and shear wave velocity for Lucknow City in Indo-Gangetic Basin. *J Pure Appl Geophys* 170(3):299–318
- BCP (2021) Building Code Of Pakistan 2021. *Ministry Of Science And Technology, Government Of Pakistan*
- Bhatti AQ, Hassan SZU, Rafi Z, Khatoun Z, Ali Q (2011) Probabilistic seismic hazard analysis of Islamabad, Pakistan. *J Asian Earth Sci* 42(3):468–478
- Bhusal B, Aaqib M, Paudel S, Parajuli HR (2022) Site specific seismic hazard analysis of monumental site Dharahara, Kathmandu, Nepal. *Geomatics Nat Hazards Risk* 13(1):2674–2696
- BSSC (2015) NEHRP Recommended Seismic Provisions for New Buildings and Other Structures, Part 1 Provisions, Part 2 Commentary, Building Seismic Safety Council. *FEMA Rept. No. P-1050-1, Washington, D.C.*

- Charney F (2015) A new linear response history analysis procedure for the 2015 NEHRP recommended provisions and for ASCE 7–16. Structures Congress 2015.
- Darendeli MB (2001) Development of a new family of normalized modulus reduction and material damping curves
- EC8 (2005) Eurocode 8: design of structures for earthquake resistance. Part 1:1998–1991
- Hashash Y, Musgrove M, Harmon J, Okan I, Groholski D, Phillips C, Park D (2017) DEEPSOIL 7.0, user manual. *University of Illinois at Urbana-Champaign*
- Hassan W, Alshameri B, Nawaz MN et al (2022) Geospatial and statistical interpolation of geotechnical data for modeling zonation maps of Islamabad, Pakistan. *Environ Earth Sci* 81:547. <https://doi.org/10.1007/s12665-022-10669-2>
- Hayashi C (1961) Theory of quantification and its examples (VI). *Proc Inst Stat Math* 9(1):29–35
- Ijaz Z, Zhao C, Ijaz N et al (2021) Spatial mapping of geotechnical soil properties at multiple depths in Sialkot region, Pakistan. *Environ Earth Sci* 80:787. <https://doi.org/10.1007/s12665-021-10084-z>
- Ijaz Z, Zhao C, Ijaz N, Rehman Z ur, Ijaz A (2022) Novel application of Google earth engine interpolation algorithm for the development of geotechnical soil maps: a case study of mega-district. *Geocarto International*, 37(27), 18196–18216. <https://doi.org/10.1080/10106049.2022.2138566>
- Ijaz Z, Zhao C, Ijaz N et al (2023) Statistical evaluation of multiple interpolation techniques for spatial mapping of highly variable geotechnical facets of soil in natural deposition. *Earth Sci Inf* 16:105–129. <https://doi.org/10.1007/s12145-022-00924-2>
- Imai T, Tonoughi K (1982) Correlation of N value with S-wave velocity and shear modulus. *Penetration Testing*
- Lee SHH (1990) Regression models of shear wave velocities in Taipei basin. *J Chin Inst Eng* 13(5):519–532
- Lodi S, Kumar M, Samad M, Wasim A (2015) Predictive relationship for estimation of V s30 using shallow bore logs for Karachi. *Geotech Geol Eng* 33(3):559–573
- Mahmood K, Farooq K, Memon SA (2016) One dimensional equivalent linear ground response analysis—a case study of collapsed Margalla Tower in Islamabad during 2005 Muzaffarabad Earthquake. *J Appl Geophys* 130:110–117
- Mahmood K, Khan SA, Iqbal Q, Karim F, Iqbal S (2020) Equivalent Linear and Nonlinear Site-Specific Ground Response Analysis of Pashto Cultural Museum Peshawar, Pakistan. *Iran J Sci Technol Trans Civil Eng*, 1–13
- Matasović N, Vucetic M (1993) Cyclic characterization of liquefiable sands. *J Geotech Eng* 119(11):1805–1822
- Mhaske SY, Choudhury D (2011) Geospatial contour mapping of shear wave velocity for Mumbai city. *Nat Hazards* 59:317–327
- Nguyen V-Q, Aaqib M, Nguyen D-D, Luat N-V, Park D (2020) A site-specific response analysis: a Case Study in Hanoi, Vietnam. *Appl Sci* 10(11):3972. <https://doi.org/10.3390/app10113972>
- Ohta Y, Goto N (1978) Empirical shear wave velocity equations in terms of characteristic soil indexes. *Earthq Eng Struct Dynamics* 6(2):167–187
- Sadiq S, Muhammad A, Mandokhail S-uJ, Rehman M-U, Mehtab A, Muhammad N, Adeel MB (2021) Evaluation of site amplification factors for shallow Rock sites of Islamabad, Pakistan. *Kuwait J Sci*, 48(2)
- Seyhan E, Stewart JP (2014) Semi-empirical nonlinear site amplification from NGA-West2 data and simulations. *Earthq Spectra* 30(3):1241–1256
- Tran N-L, Aaqib M, Nguyen B-P, Nguyen D-D, Tran V-L, Nguyen V-Q (2021) Evaluation of seismic site amplification using 1D site response analyses at Ba Dinh Square Area, Vietnam. *Adv Civil Eng* 2021:1–11

**Publisher's Note** Springer Nature remains neutral with regard to jurisdictional claims in published maps and institutional affiliations.

Springer Nature or its licensor (e.g. a society or other partner) holds exclusive rights to this article under a publishing agreement with the author(s) or other rightsholder(s); author self-archiving of the accepted manuscript version of this article is solely governed by the terms of such publishing agreement and applicable law.